Available online at www.sciencedirect.com
SCIENCE DIRECT®
Pergamon
Materials Research Bulletin 38 (2003) 1063–1072
Materials Research Bulletin
www.elsevier.com/locate/matresbu

Synthesis, characterization and electrical properties of quaternary selenodiphosphates: AMP_2SE_6 with A = Cu, Ag and M = Bi, Sb

A. Galdámez[a], V. Manríquez[a,*], J. Kasaneva[b], R.E. Avila[c]

[a]*Departamento de Química, Facultad de Ciencias, Universidad de Chile, Casilla 653, Santiago, Chile*
[b]*Universidad de Antofagasta, Facultad de Ciencias Básicas, Antofagasta, Chile*
[c]*Departamento de Investigación y Desarrollo, Comisión Chilena de Energía Nuclear, Casilla 188-D, Santiago, Chile*

Received 3 January 2003; received in revised form 3 February 2003; accepted 12 February 2003

Abstract

The new quaternary selenophosphate phases AMP_2Se_6 (A = Cu, Ag and M = Bi, Sb) were synthesized by ceramic methods at 1023 K. These phases were characterized by powder X-ray diffraction (XRD), Fourier transform infrared spectroscopy (FTIR), energy dispersive X-ray analysis (EDX) and a.c. and d.c. electrical conductivity measurements. The phases all show values of electrical conductivity, σ, of about $10^{-4}\,\Omega^{-1}\,cm^{-1}$ at 303 K and photoconductive effect. The conductivity is nearly five orders of magnitude larger than that of related phases.

Keywords: D. Electrical properties; A. Layered compounds

1. Introduction

The study of compounds in the family of $M_2P_2Q_6$ (M = Mn, Fe, Co, Ni, Cd, V, Mg, Pb, Hg, Sn; Q = S, Se), has been stimulated because of their highly anisotropic physical properties, useful for possible applications in electrooptical devices. The first layered selenodiphosphate synthesized, $Fe_2P_2Se_6$, was reported by Klingen et al. in 1973 [1]. In the layered structure of this material, the transition metal cation Fe^{2+} and the P–P pairs, occupy the octahedral holes between the planes of selenium atoms. The substitution of the cations M^{2+}, by M^{1+} (Ag, Cu) and M^{3+} (such as Cr, In, V, Ga, Sc) results in thermodynamically stable quaternary chalcophosphates with structures of the $CdCl_2$ type [2].

The selenodiphosphate compounds containing Bi and Sb, have been synthesized by solid state reaction of the elemental powders at low temperature. The phases $M_4(P_2Se_6)_3$ (M = Bi, Sb) exhibit structures related to $Pb_2P_2Se_6$ [3], while the phase β-$Bi_4(P_2Se_6)_3$ exhibits a three-dimensional (3D)

* Corresponding author. Tel.: +56-2-6787-251; fax: +56-2-2713-888.
E-mail address: vmanriqu@abello.dic.uchile.cl (V. Manríquez).

0025-5408/03/$ – see front matter
doi:10.1016/S0025-5408(03)00068-0

structure, with groups $BiSe_8$ and $P_2Se_6^{4-}$ [4]. The quaternary selenodiphosphates KMP_2Se_6 and $Cs_8M_4(P_2Se_6)_5$ (M = Bi, Sb) have been synthesized using low temperature methods [5]. The phases KMP_2Se_6 are isostructural and exhibit two-dimensional (2D) structures. The phases $Cs_8M_4(P_2Se_6)_5$ present tunnels interconnected by M···M interactions in a 2D structure. An important characteristic of the Bi and Sb atoms, in solid phases, is the stereochemical localization of the ns^2 electron pairs, which produces important variations in crystal structure, physical properties and electronic structure of the resulting materials.

In this work, we report the synthesis, characterization and electrical properties of the new phases AMP_2Se_6 (A = Cu, Ag; M = Bi, Sb), which are structurally related to $Fe_2P_2S_6$. As far as we know, up to now, these phases are the first quaternary compounds of Bi and Sb that contain a transition metal counterion (A^{1+}).

2. Experimental section

2.1. Synthesis

The phases AMP_2Se_6 (A = Cu, Ag; M = Bi, Sb) were synthesized by two sets of experimental conditions. In both, the reaction mixtures were sealed in evacuated quartz ampoules, and heated at 1023 K for 1 week. In the first method, the compounds were obtained by direct combination of the pure elements in stoichiometric proportions, with an excess of selenium and phosphorus (1% mass) to avoid the formation of impurity phases (Cu_3PSe_4, $Ag_4P_2Se_6$ and M_2Se_3). Homogeneous and well-crystallized materials were obtained after grinding and reheating at 1023 K for 1 week. SEM-EDX analyses carried out on the samples confirmed their purity, homogeneity and stoichiometry (Table 1). In the second procedure, the synthesis proceeded by direct combination of the pure elements with an excess of P_2Se_5 and Se, so that all of the metal reacted to give well-crystallized products. A, M, P_2Se_5, and Se were mixed in molar ratios 1:1:1.5:2.0. After the reaction was completed, the reacted matter was slowly cooled to room temperature at the rate of 6 K/h. The reaction mixture was washed with DMF/ethylenediamine (3:1) to remove the P_ySe_z and Se. The product was washed with anhydrous ether and consisted of black laminar crystals. EDX analysis carried out on the resulting crystals indicated an average composition of $Cu_{1.0}Bi_{1.0}P_{1.8}Se_{6.1}$.

2.2. Characterization

XRD data were collected at room temperature on a Siemens D 5000 powder diffractometer, with Cu Kα radiation in the range $5 < 2\theta < 80$. The lattice parameters were calculated from least-square fits

Table 1
Analytical data (% w/w) for the AMP_2Se_6 phases

Cu	Ag	Bi	Sb	P	Se	Proposed formula
7.8	–	25.7	–	7.3	59.2	$CuBiP_2Se_6$
–	13.2	24.2	–	7.2	55.4	$AgBiP_2Se_6$
10.0	–	–	16.5	8.2	65.3	$CuSbP_2Se_6$
–	14.3	–	16.1	7.8	61.8	$AgSbP_2Se_6$

using the Powder Diffraction Package (PDP) and Powder Pattern Lattice Parameter (PPLP) refinement routine of the NRCVAX program. For electron microscopy, analyses were performed on a JEOL 6400 scanning electron microscopy (SEM) equipped with Oxford Link Isis energy dispersive X-ray (EDX) detector. The average A:M:P:Se elemental ratio of all samples was 1:1:2:6.

Differential Thermal Analysis (DTA) and Thermogravimetric Analysis (TG) were performed on a Rheometric Scientific STA 1500H/625 Thermal Analysis System. The DTA/TG curves were run simultaneously on each sample from room temperature to 1273 K, in flowing nitrogen at a heating rate of 10 K/min. Infrared spectra were recorded on a BRUKER VECTOR 22 with Fourier transform SJ-IR spectrometer in the spectral range 250–600 cm^{-1}. The spectra of the powders were recorded in polyethylene pellets. Magnetic susceptibility (χ) measurements were performed on polycrystalline samples between 5 K and room temperature under a constant field strength of 1 kG, using a SHE VTS-906 SQUID detection system. The electrical conductivity was measured by a.c. and d.c. methods. The two opposite flat surfaces of the samples were sputtered with gold and sandwiched between the platinum electrodes of the conductivity cell. Impedance measurements were carried out with a Solartron SI-1260 impedance gain-phase analyzer in the frequency range 0.1–10 MHz with a signal level between 25 mV and 1 V, to probe the charge transport mechanism. Direct current measurements were performed with a Keithley 237 source-meter, to ascertain the existence of slow relaxation mechanisms that may not be accessible through the impedance measurements. Photoconductivity measurements were carried out in the temperature range 296–473 K, and pressure of approximately 10^{-3} atmosphere. The samples, pressed into cylindrical disks, were mounted in a metallic holder, where illumination could be achieved through a transparent window. The light power density was 50 mW/cm^2 from a Doolan Jenner Fiberlite A3200 halogen lamp. The current was recorded with a programmable Keithley 617 electrometer with silver paint contacts and planar configuration of the electrodes. The *I–V* curves were verified to be linear, supporting the Ohmic character of the contacts.

3. Results and discussion

The indexing of the X-ray powder diffractograms shows that the phases AMP_2Se_6 belong to the space group *C*2/*m* and their structures are related to that of $Fe_2P_2S_6$. The phases AMP_2Se_6 present a 2D structure and they can be regarded as a substitution of Fe^{2+}, in the $Fe_2P_2S_6$ layer, by the cations A^{1+} and M^{3+}. The observed and calculated interplanar spacing (d_{hkl}) and the unit cell constants are shown in Tables 2 and 3, respectively. The 0 0 1 interplanar *d*-spacing shows that the phases correspond to unintercalated layer compounds. The infrared spectrum shows a strong absorption at 428 cm^{-1} in $CuBiP_2Se_6$, 430 cm^{-1} in $AgBiP_2Se_6$, 432 cm^{-1} in $CuSbP_2Se_6$ and 429 cm^{-1} $AgSbP_2Se_6$. This vibration can be assigned to the asymmetric stretching (νPSe_3), indicating the presence of $P_2Se_6^{4-}$ units in the structure. Both IR and XRD results indicate that the metals A^{1+} and M^{3+} were incorporated, rather than intercalated, into the layer of the phases AMP_2Se_6. Quaternary phases of bismuth and antimony reported in the literature also possess layer structures. The phase KMP_2Se_6 (M = Sb, Bi) contains K^+ intercalated in the interlayer space of lamellar $MP_2Se_6^{1-}$, where $Cs_8M_4(P_2Se_6)_5$ (M = Bi, Sb) present a staircase layered structure with tunnels along the *b* direction, Cs^{1+} is found in the tunnels and within the layer.

DTA/TG showed a slight weight loss of approximately 2% between 523 and 673 K, which may be assigned to partial selenium loss, and a decomposition peak at 803 K with a weight loss of 23.8%. The XRD of the residues indicated the presence of M_2Se_3 and A_2Se.

Table 2
Observed and calculated Powder Diffraction data

$CuBiP_2Se_6$					$AgBiP_2Se_6$				
2θ	Int	d_{cal}	d_{obs}	$h\,k\,l$	2θ	Int	d_{cal}	d_{obs}	$h\,k\,l$
13.58	100	6.51	6.51	0 0 1	13.50	100	6.56	6.55	0 0 1
17.29	3	5.13	5.13	1 1 0	16.80	1	5.28	5.27	0 2 0
18.83	6	4.708	4.708	−1 1 1	17.87	1	4.96	4.96	1 1 0
20.86	1	4.256	4.256	0 2 1	19.12	1	4.641	4.637	−1 1 1
27.12	58	3.285	3.285	0 0 2	20.84	3	4.262	4.259	0 2 1
29.65	4	3.011	3.011	−2 0 1	24.39	1	3.649	3.647	1 1 1
30.67	26	2.913	2.913	−1 3 1	27.08	42	3.292	3.289	0 0 2
31.77	2	2.814	2.814	0 2 2	27.42	11	3.253	3.250	−1 1 2
32.42	2	2.759	2.759	0 4 0	29.82	9	2.996	2.993	−2 0 1
38.82	16	2.138	2.138	−2 2 2	30.18	19	2.961	2.959	2 0 0
39.55	1	2.277	2.277	−1 1 3	32.52	1	2.755	2.753	0 2 2
40.62	3	2.219	2.219	2 2 1	33.29	1	2.692	2.689	0 4 0
41.05	23	2.197	2.197	0 0 3	38.48	10	2.340	2.337	−2 2 2
48.26	5	1.884	1.884	−2 4 2	39.67	11	2.272	2.270	2 2 0
49.93	9	1.825	1.825	2 2 2	41.05	19	2.199	2.197	0 0 3
51.00	3	1.789	1.789	−3 3 1	44.69	1	2.028	2.026	0 2 3
55.60	41	1.652	1.651	0 0 4	45.41	2	1.997	1.995	2 4 0
57.45	1	1.603	1.603	−2 2 4	49.71	7	1.834	1.832	2 2 2
58.81	2	1.569	1.569	−2 6 1	55.67	23	1.651	1.648	0 0 4
60.25	1	1.5349	1.5347	−4 0 2	60.63	1	1.5272	1.5250	2 6 0
61.22	1	1.5129	1.5129	2 2 3	62.80	2	1.4797	1.4782	4 0 0
65.69	2	1.4203	1.4202	1 7 1	67.42	1	1.3890	1.3887	3 3 2
71.07	1	1.3253	1.3250	−2 2 5	70.91	2	1.3290	1.3285	−4 4 2
76.53	3	1.2439	1.2439	0 8 2	76.14	1	1.2502	1.2516	2 2 4
77.74	6	1.2274	1.2274	−2 8 1	77.70	4	1.2289	1.2288	−5 1 2
					79.07	2	1.2111	1.2107	−3 3 5
$CuSbP_2Se_6$					$AgSbP_2Se_6$				
13.63	50	6.49	6.49	0 0 1	13.36	100	6.62	6.62	0 0 1
17.21	1	5.15	5.15	1 1 0	16.92	3	5.23	5.23	1 1 0
19.31	2	4.594	4.594	−1 1 1	21.53	2	4.125	4.124	0 2 1
19.62	1	4.521	4.520	0 2 1	26.85	64	3.318	3.317	0 0 2
24.17	1	3.679	3.679	1 1 1	30.31	13	2.946	2.946	2 0 0
27.17	100	3.280	3.279	0 0 2	31.23	3	2.861	2.861	0 2 2
27.76	5	3.212	3.211	−1 1 2	34.17	4	2.622	2.621	−2 0 2
29.68	2	3.008	3.008	−2 0 1	35.71	2	2.512	2.512	1 1 2
30.89	23	2.892	2.892	−1 3 1	37.21	3	2.414	2.414	−2 2 2
31.86	1	2.806	2.805	0 2 2	40.17	17	2.243	2.214	−1 1 3
34.44	2	2.602	2.601	−2 0 2	41.40	3	2.179	2.179	0 0 3
39.02	12	2.306	2.306	−2 2 2	43.73	4	2.068	2.068	0 2 3
39.85	3	2.260	2.263	−1 1 3	47.83	6	1.900	1.901	−1 3 3
41.07	8	2.196	2.196	0 0 3	49.50	8	1.836	1.836	2 2 2
44.27	1	2.045	2.044	0 2 3	51.55	3	1.772	1.771	3 3 0
46.00	1	1.972	1.972	−1 5 1	55.24	22	1.661	1.661	−2 0 4
48.73	6	1.867	1.867	1 1 3	57.65	3	1.598	1.597	−2 2 4
50.11	11	1.819	1.818	2 2 2	62.59	2	1.4828	1.4828	4 0 0
55.63	28	1.651	1.650	0 0 4	63.97	2	1.4541	1.4541	−3 5 2

Table 2 (*Continued*)

$CuBiP_2Se_6$					$AgBiP_2Se_6$				
2θ	Int	d_{cal}	d_{obs}	$h\,k\,l$	2θ	Int	d_{cal}	d_{obs}	$h\,k\,l$
63.19	2	1.4703	1.4702	−2 6 2	69.16	2	1.3572	1.3571	3 5 1
65.34	2	1.4271	1.4272	4 2 0	75.97	1	1.2515	1.2514	2 2 4
76.75	2	1.2408	1.2407	0 8 2	77.39	3	1.2321	1.2321	−3 5 4
77.86	7	1.2259	1.2258	−2 8 1					
79.49	2	1.2047	1.2047	−3 7 2					

Table 3
Lattice parameters

Phase	a (Å)	b (Å)	c (Å)	β (°)	V (Å^3)
$CuBiP_2Se_6$	6.19 (2)	10.73 (2)	6.94 (2)	107.46 (6)	439.37
$AgBiP_2Se_6$	6.20 (2)	10.71 (3)	6.90 (2)	107.20 (7)	437.55
$CuSbP_2Se_6$	6.16 (2)	10.71 (4)	6.89 (2)	106.48 (6)	436.13
$AgSbP_2Se_6$	6.20 (2)	10.73 (3)	6.90 (2)	107.34 (9)	437.88

Magnetic measurements carried out on $CuSbP_2Se_6$ showed temperature-independent paramagnetism. The calculated magnetic moment is 0.19 BM, which could be related to non-stoichiometry in the Cu sublattice.

The compounds AMP_2Se_6 are semiconductors with electrical conductivity, σ, of about $10^{-4}\ \Omega^{-1}\ cm^{-1}$ at 303 K (Table 4). These values are much larger than those of the related compounds $Cs_8M_4(P_2Se_6)_5$ (M = Sb, Bi). Thus, $Cs_8Sb_4(P_2Se_6)_5$ and $Cs_8Bi_4(P_2Se_6)_5$ are insulatings, the bismuth compound shows electrical conductivity of $\sigma = 10^{-9}\ \Omega^{-1}\ cm^{-1}$ at room temperature [5b]. From the above results, it appears that the presence of the cations Ag^+ and Cu^+ in AMP_2Se_6 is responsible for this large increase in electrical conductivity.

The a.c. impedance measurements give typical depressed semicircular plots (Nyquist diagrams), suggesting the presence of wide distributions of relaxation times. Fig. 1 shows representative plots of $CuBiP_2Se_6$ and $AgBiP_2Se_6$ (parts a and b, respectively) measured at room temperature. By fitting discrete elements models [6,7] it is possible to identify the resistance and effective capacitance corresponding to the single arc, resulting in the values reported in Table 5. The values of the effective capacitance suggest that the electrical conductivity in these AMP_2Se_6 compounds is controlled by the intergranular transport. The Nyquist plot resulting from $AgBiP_2Se_6$ has been singled out in Fig. 1b, as it

Table 4
Dark conductivity (σ_d) and photoconductivity (σ_{ph}) at 303 K

Phase	σ_d ($\Omega^{-1}\ cm^{-1}$)	σ_{ph} ($\Omega^{-1}\ cm^{-1}$)	σ_{ph}/σ_d
$CuBiP_2Se_6$	1.46×10^{-4}	1.94×10^{-4}	1.33
$AgBiP_2Se_6$	6.34×10^{-4}	6.59×10^{-4}	1.04
$CuSbP_2Se_6$	4.56×10^{-5}	5.96×10^{-5}	1.20
$AgSbP_2Se_6$	1.45×10^{-4}	1.65×10^{-4}	1.14

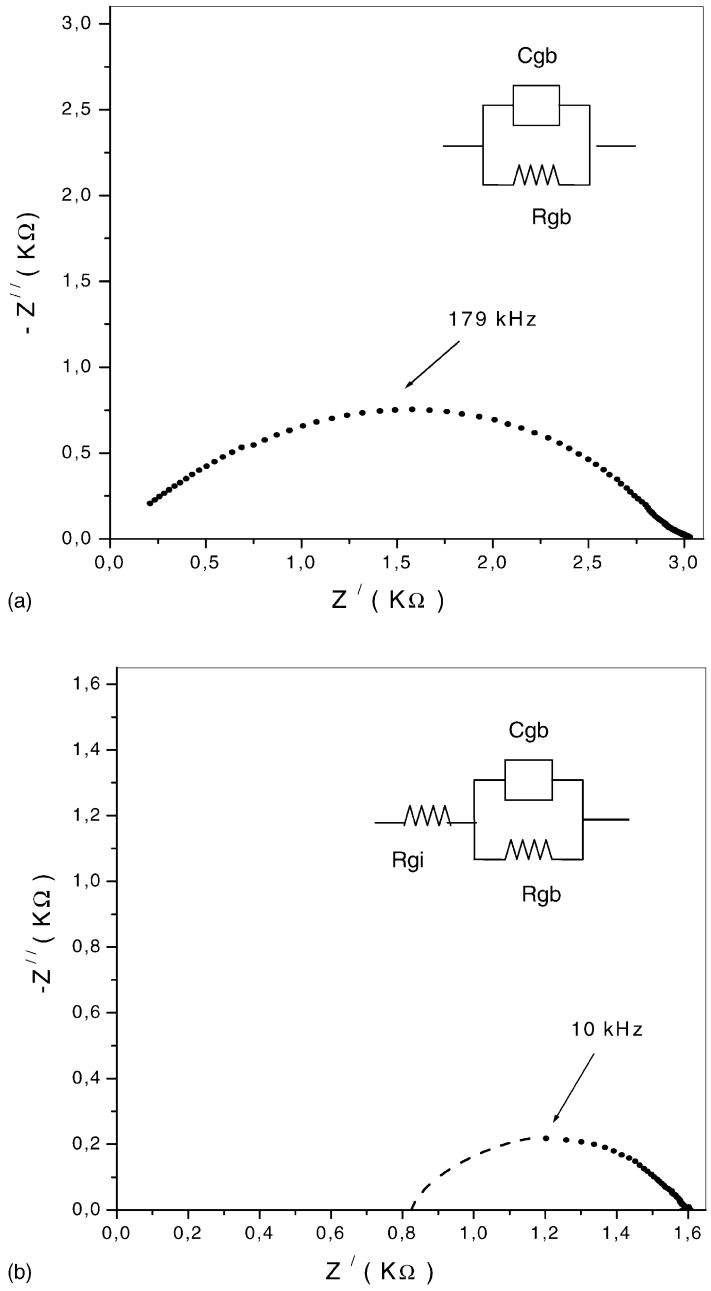

Fig. 1. Impedance complex plane plot of (a) $CuBiP_2Se_6$, (b) $AgBiP_2Se_6$.

is the only one to deviate noticeably from the single depressed arc going through the origin behaviour. Indeed, the arc, which starts out at the maximum frequency available from the experimental system, is displaced from the origin. The series combination of a resistance (R_{gi}) with the parallel combination of a resistance (R_{gb}) and a constant phase element (C_{gb}) fits the data. The resistance R_{gi}, which causes the

Table 5
Resistance and effective capacitance calculated from the Nyquist curves

Phase	Temperature (K)	R_{gb} (Ω)	C_{gb} (F)
$CuBiP_2Se_6$	293	3040	3.01×10^{-10}
$AgBiP_2Se_6$	288	R_{gi}: 864, R_{gb}: 1593	7.10×10^{-11}
$CuSbP_2Se_6$	295	17890	1.93×10^{-11}
$AgSbP_2Se_6$	297	3125	3.20×10^{-11}

displacement, is 864 Ω and the second, defining the arc diameter, is 729 Ω. The value of the effective capacitance, 71 pF, in the latter element, suggests control by intergranular transport, as in the other samples, however, the displacement represented by R_{gi} suggests that an arc due to intragrain transport may be active at higher frequency than registered. Both these values of the resistance are reported in Table 5, leading to an effective d.c. resistance of 1593 Ω.

The d.c. electrical conductivity measurements show the characteristic behavior of photoconductive materials [8]. Fig. 2 shows the current as a function of time, where a monotonic rise to a steady value can be observed upon illumination, followed by quite a slow decay of the photoconductivity upon removal of the illumination source. A persistent photoconductivity effect is observed in $AgBiP_2Se_6$ after turning off the illumination. This type of photoconductivity behavior has been reported in chalcogenide glasses and intercalated chalcogenides [9]. In all of the cases where thermally activated behavior is observed, the experimental data correlate with the expression:

$$\sigma = \sigma_0 \exp\left(\frac{-E_a}{kT}\right)$$

where σ_0 is a constant, E_a is the activation energy, k is Boltzmann's constant and T is the absolute temperature.

The temperature dependence of the d.c. conductivity presents approximately Arrhenius behavior in the temperature range of the measurements, as indicated in Fig. 3. In all four phases, the dark conductivity increases as the temperature rises. This behavior is consistent with the thermal activation of trapped carriers in a wide-gap semiconductor material. The corresponding activation energies are collected in Table 6. Both dark conductivity σ_d and photoconductivity σ_{ph} are thermally activated, in the whole temperature range investigated. In the phases AMP_2Se_6 studied, those with A = Cu show greater photosensitivity (σ_{ph}/σ_d) than those with A = Ag (Table 4).

Table 6
Activation energy and temperature range of dark conductivity and photoconductivity

Phase	Temperature range (K)	E_a (eV)
Dark conductivity		
$AgBiP_2Se_6$	303–375	0.06
$AgSbP_2Se_6$	328–373	0.29
$CuSbP_2Se_6$	303–403	0.15
$CuBiP_2Se_6$	303–463	0.14
Photoconductivity		
$CuBiP_2Se_6$	303–463	0.10

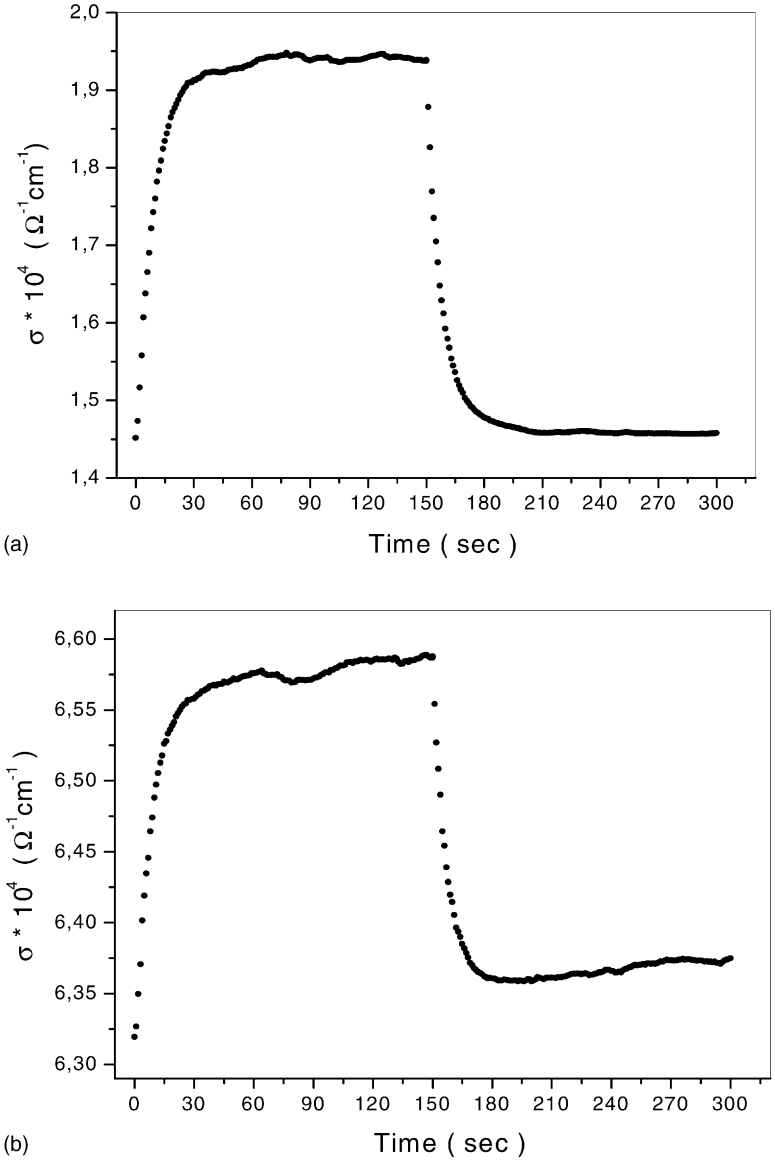

Fig. 2. Direct current photoconductivity as a function of time: (a) $CuBiP_2Se_6$, (b) $AgBiP_2Se_6$.

For interpreting the photoconductivity in the phases AMP_2Se_6, we have used an extended Huckel (EH) calculation scheme based on the crystal structure reported for $CuCrP_2Se_6$, isostructural with $Fe_2P_2S_6$ [2a]. In these schemes, the highest energy valence bands are derived from the (P–P) p bonding orbitals, from (Se) p nonbonding orbitals and from (P–Se) p hybridized orbitals. The lowest energy conduction bands are generated by the (Cu) s bonding orbitals, the (P–P) p antibonding and (Se) p bonding states. The (Bi) s orbitals are below the main valence band. The exposure of the sample to light produces holes in the (Se) p valence nonbonding band and electrons in the (Cu) s conduction bonding band. The free centers in the (P–P) p valence bonding band act as recombination centers.

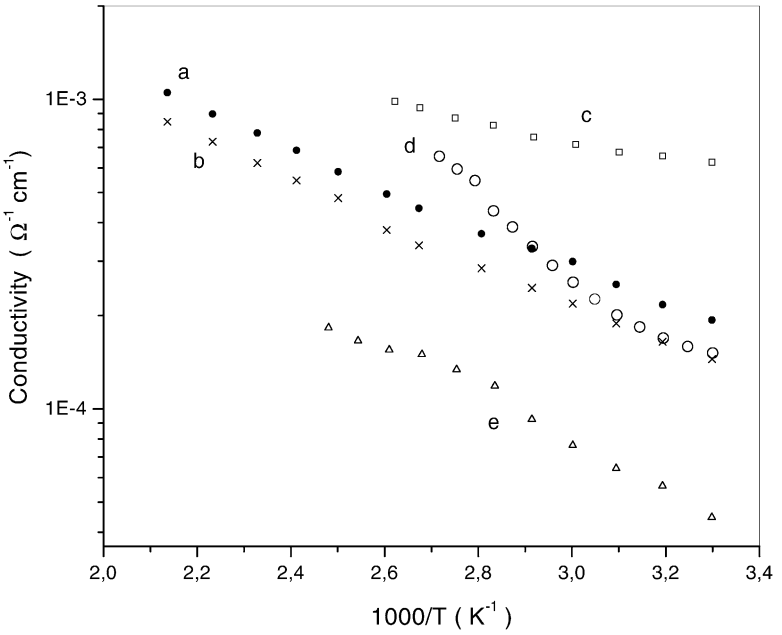

Fig. 3. Direct current dark conductivity and photoconductivity as a function of temperature: (a) photoconductivity of $CuBiP_2Se_6$, (b) dark conductivity of $CuBiP_2Se_6$, (c) dark conductivity of $AgBiP_2Se_6$, (d) dark conductivity of $AgSbP_2Se_6$ and (e) dark conductivity of $CuSbP_2Se_6$.

Acknowledgements

We thank Dr. Octavio Peña at the Laboratoire du Chimie du Solide et Inorganique Moléculaire, Université du Rennes 1/FRANCE, for the magnetic susceptibility measurements and Dr. Fernando Mendizábal at Facultad de Ciencias, Universidad de Chile for the band structure calculations. This work was supported by FONDECYT through operating grants no. 1020683 and ''Beca Apoyo de Tesis 2002''.

References

[1] W. Klingen, G. Eulenberg, H. Hand, Z. Anorg. Allg. Chem. 431 (1973) 97.
[2] (a) R. Pfeiff, R. Kneip, J. Alloys Compd. 186 (1992) 111;
(b) R. Brec, G. Ouvrard, A. Louisy, J. Rouxel, A. Le Mehauté, Solid State Ionics 6 (1982) 185;
(c) S. Lee, P. Colombet, G. Ouvrard, R. Brec, Inorg. Chem. 27 (1988) 1291;
(d) Y. Mathey, R. Clement, J.P. Audiere, O. Poizat, C. Sourisseau, Solid State Ionics 9/10 (1983) 456;
(e) V. Maisonneuve, V.B. Cajipe, Phys. Rev. 17 (1997) 10860.
[3] M. Ruck, Z. Anorg. Allg. Chem. 621 (1995) 1344.
[4] J. Aitken, S. Brown, K. Chondroudis, S. Jobic, R. Brec, M. Kanatzidis, Inorg. Chem. 38 (1999) 4795.
[5] (a) T. McCarthy, M. Kanatzidis, J. Chem. Soc. Chem. Commun. 9 (1994) 1089;
(b) T. McCarthy, T. Hogan, C. Kannnewurf, M. Kanatzidis, Chem. Mater. 6 (1994) 1072.
[6] J.T.S. Irvine, D.C. Sinclair, A.R. West, Adv. Mater. 2 (1990) 132.

[7] J.R. Macdonald, Impedance Spectroscopy, Wiley, 1987.
[8] (a) A. Carnabuci, V. Grasso, L. Silipingni, G. Salvato, J. Appl. Phys. 90 (2001) 4536;
(b) V. Grasso, F. Neri, S. Santangelo, L. Silipigni, M. Piacentini, Phys. Rev. B 37 (1988) 4419.
[9] (a) S. Goel, A. Kumar, Thin Solid Films 151 (1987) 307;
(b) V. Manríquez, A. Galdámez, J. Ponce, I. Brito, J. Kasaneva, Mater. Res. Bull. 34 (1999) 123.